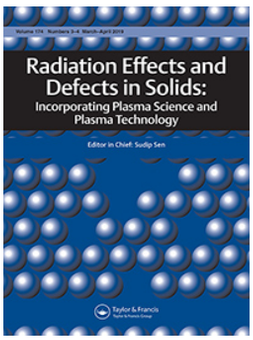

Taylor & Francis
Taylor & Francis Group

Radiation Effects and Defects in Solids

Incorporating Plasma Science and Plasma Technology

ISSN: 1042-0150 (Print) 1029-4953 (Online) Journal homepage: https://www.tandfonline.com/loi/grad20

The effects of multicharged ion irradiation on a polycarbonate surface

E. S. Srinadhu, D. D. Kulkarni, D. A. Field, J. E. Harriss & C. E. Sosolik

To cite this article: E. S. Srinadhu, D. D. Kulkarni, D. A. Field, J. E. Harriss & C. E. Sosolik (2019) The effects of multicharged ion irradiation on a polycarbonate surface, Radiation Effects and Defects in Solids, 174:3-4, 205-213, DOI: 10.1080/10420150.2018.1552958

To link to this article: https://doi.org/10.1080/10420150.2018.1552958

Published online: 04 Jan 2019.

RADIATION EFFECTS & DEFECTS IN SOLIDS
2019, VOL. 174, NOS. 3–4, 205–213
https://doi.org/10.1080/10420150.2018.1552958

Taylor & Francis
Taylor & Francis Group

The effects of multicharged ion irradiation on a polycarbonate surface

E. S. Srinadhu [a], D. D. Kulkarni[b], D. A. Field[c], J. E. Harriss [c] and C. E. Sosolik [c]

[a]Lam Research Corporation, Fremont, CA 94538; [b]Verseon Corporation, Fremont, CA 94538; [c]Department of Physics and Astronomy, Clemson University,Clemson, South Carolina, 29634

ABSTRACT

Polycarbonate targets were irradiated with multicharged ions of argon and oxygen with kinetic energies between 375 eV and 1 keV. Scanning electron microscopy (SEM) and x-ray photoelectron spectroscopy (XPS) analysis following the irradiations showed evidence of bond-breaking at the polycarbonate surface. The extent of the ion-induced damage indicates that the ion charge state enhances the damage well beyond that observed for similar, low flux singly charged ions. A qualitative comparison with a simple description of the radius of capture for the initial transfer of electrons between the ion and surface is used to understand the multicharged ion effects.

ARTICLE HISTORY
Received 3 April 2018
Accepted 16 November 2018

KEYWORDS
Multicharged ions; polycarbonate; XPS

1. Introduction

Ion beam processing methods traditionally rely on an ion's kinetic energy to effect material modifications. This is particularly true at surfaces, where the typical interaction cross section (10^{-16} cm^2) is such that a fluence comparable to or exceeding the surface density is used (*1*, *2*, *3*, *4*). In other words, the fluence-to-density equivalence indicates that the ions, almost always singly charged, collide with and modify a surface through nuclei-nuclei collisions. Although the electrons of a singly-charged ion (SCI) participate in the collision, they primarily serve as a partial screen of the ion's nuclear charge (*5*, *6*, *7*, *8*, *9*) and as a minor channel for charge exchange between the ion and the target material (*10*, *11*). In some cases, damage introduced by the electronic stopping of an impacting SCI can give rise to significant and measurable effects, such as those seen in ion-stimulated desorption on alkali halides(*12*). Enhanced desorption effects for ions that are missing multiple electrons and arrive at a surface as a multicharged ion (MCI) have also been seen, such as the case of MCIs and proton desorption (*13*, *14*, *15*, *16*). In general, these MCIs are of interest because the summed binding energies of their missing electrons (reneutralization energy) can become comparable to the their kinetic energy, and this can govern the type of material modifications initiated by the ion impact (*17*, *18*, *19*, *20*) or be used to tune modification on certain substrates (*21*, *22*).

Previous efforts aimed at utilizing the stored potential energy of MCIs to initiate chemistry have already shown that nano-patterning is possible, since each ion dissipates its

CONTACT C. E. Sosolik sosolik@clemson.edu

energy within a small, nanometer-sized volume during the target interaction (*19*, *20*, *23*). This is in contrast to the long, subsurface track formation that results from impacts of SCIs that have comparable energies (*24*, *25*). This distinction between the dissipation of potential and kinetic energy for MCIs and SCIs is clearly visible in terms of the highly surface-specific effects that MCIs can initiate, e.g. nanhillock/nanocrater formation (*19*, *26*), potential sputtering (*27*, *28*) and enhanced desorption (*18*, *29*, *30*, *31*).

Specific measurements that utilize MCIs to irradiate polycarbonate (PC) have been largely confined to high kinetic energies (MeV range) where post-processing through etching has been used. These studies have typically been done in the low dose limit (10^8 - 10^{10} cm^{-2}) to avoid overlapping of impact sites after etching (*32*, *33*, *34*, *35*). A primary focus of those efforts was the formation and subsequent study of pores in the polycarbonate that are the result of the passage of the MCIs through the target. In these cases, the equilibrium stopping force inside the target is an important factor; however, we are focused here instead on the role of ion modifications at the surface only, which means the incident charge state will be the controlling factor. In our prior studies with MCIs, we have utilized encapsulation of damaged targets within electronic devices, e.g. capacitors, to probe subsurface irradiation effects. As PC does not lend itself to such encapsulation, we have opted for x-ray photoelectron spectroscopy (XPS), which is a surface-sensitive technique. Using XPS, we investigate the charge- or Q-dependent ability of MCIs to break the surface bonds of our polycarbonate targets. This differs somewhat from current ion-based processing of polycarbonate, which rely on a high dose of SCIs that is often coupled with an in-situ flow of oxygen to facilitate crosslinking at the surface. This processing can improve the polycarbonate adhesion, as evidenced through both contact angle and x-ray photoelectron spectroscopy (XPS) data (*2*, *36*, *37*, *38*, *39*, *40*). Our data show that the extracted measures of damage observed for MCI radiation can exceed those seen for SCIs on a per ion basis even in the absence of oxygen flow and that the scale of that damage is Q-dependent.

In Section 2 we detail our sample preparation, ion irradiation and post-irradiation spectroscopy procedures. The results of these experiments, including a discussion of the charge state dependence seen in the data, are presented in Section 3. A summary is given in Section 4.

2. Experiment

Measurements were carried out using samples obtained from a single sheet of commercially available polycarbonate (Lexan, US Plastics). Specifically, the polycarbonate sheet was diced to create square samples each with an area of approximately 100 mm^2. Each diced sample was rinsed with DI water, isopropyl alcohol and ethanol before ion irradiation. The sample irradiations with MCIs were carried out using ions obtained from the EBIS-SC ion source at the CUEBIT laboratory at Clemson University (*41*). Ions were delivered through a beamline attached to the source that is kept at a pressure in the low 10^{-9} Torr range to avoid neutralization from charge exchange with residual gases.

The ion species used were O^{3+}, O^{5+} and Ar^{8+}, which have potential energies of 103 eV, 290 eV and 567 eV respectively. These charge state and species combinations were transported through the beamline at high kinetic energy, filtered according to their charge-to-mass ratio using an analyzing dipole magnet and then delivered to a target chamber region (base pressure 10^{-8} Torr). Within the target chamber, the ions were decelerated and

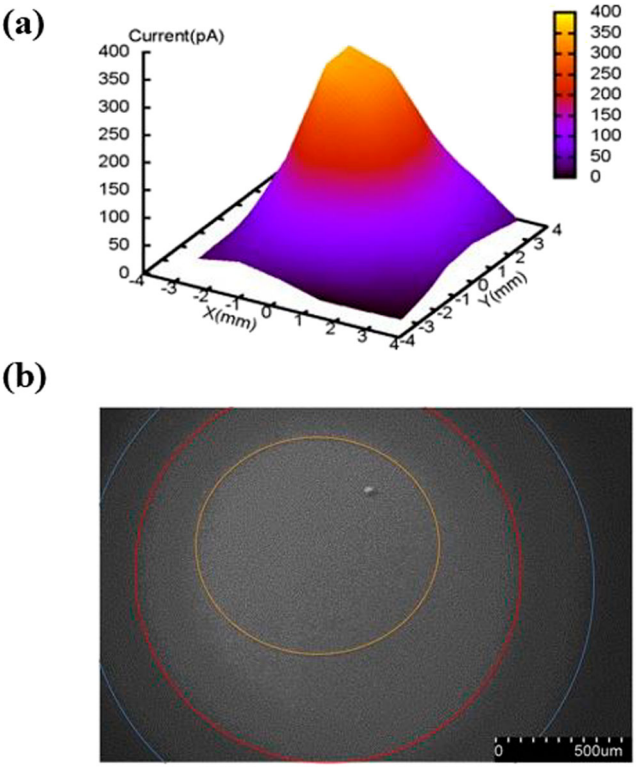

Figure 1. a) Profile of a 375 eV O^{5+} beam obtained by translating the target Faraday cup in the sample plane. b) An SEM image of a polycarbonate sample following irradiation by the O^{5+} beam at a dose of 4.95×10^{12} cm^{-2}. The color scale (shown as ellipses in (b)) has been mapped onto that used for the profile of (a) to highlight the beam irradiation zone on the sample surface.

focused onto the polycarbonate samples at normal incidence. Each sample was exposed to a specific ion species at low kinetic energy (0.375 - 1.0 keV). Beam currents were measured by a Faraday cup mounted in the same plane as the sample, and spatial profiles of the beam were obtained by translating the Faraday cup in this plane. The profiles showed the beams to be approximately Gaussian in shape with $\sim$ 3 mm FWHM. A typical beam profile is shown in Figure 1 for O^{5+} ions along with a scanning electron microscope (SEM) image of a polycarbonate sample region exposed to the beam. The SEM image was obtained on a Hitachi S4800 operating in variable pressure mode using a backscattered electron detector. The total ion dose used in these measurements was in the range of 10^{12} - 10^{13} ions per cm^2.

Following irradiation of the polycarbonate samples, XPS measurements were used to track charge- and dose-dependent changes in the chemical composition induced by the MCIs. The XPS measurements were made using a Kratos Axis Ultra (K_α, $h\nu = 1486.6$ eV) at the Georgia Tech Institute for Electronics and Nanotechnology. Figure 2(a,b) show C-1s spectra for pristine and irradiated samples, respectively, while the inset shows the chemical structure of polycarbonate. All C-1s spectra were fit to a Gaussian/Lorentzian mixed model after applying a background subtraction and corrections for charging effects, and

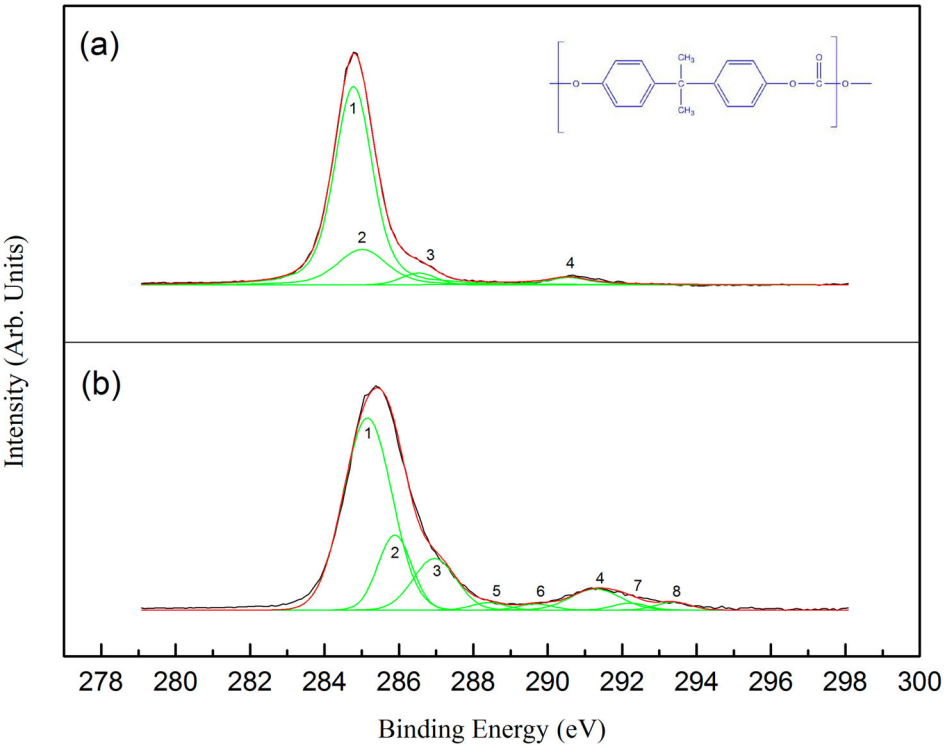

Figure 2. XPS spectra obtained on (a) pristine and (b) irradiated polycarbonate samples. The irradiated sample was exposed to 1000 eV Ar^{8+} ions with a dose of 1.41×10^{12} cm^{-2}.

Table 1. Polycarbonate structure and bond assignments notated by assigned XPS peak number(s).

Peak	Polycarbonate Structure
1	Aromatic C-C/C-H
2	Aliphatic C-C/C-H
3	Aromatic C-O
4	Carbonate O-(C = O)-O
5	Aliphatic C = O
6	O-C = O
7-8	$\pi - \pi$ satellites

example fits are shown in Figure 2. The peaks labeled here can be correlated to particular polycarbonate structures or bonds, as indicated in Table 1.

For our experiments, multiple C-1s and O-1s spectra were recorded on each irradiated sample by translating the sample in 250 μm steps across the center of the irradiated region, where the radius of a typical XPS-sampled area was 30 μm. Any spatial variation observed could be attributed to the MCI beam profile (see e.g. Figure 1(a)), and only those spectra corresponding to the central 1-2 mm of the irradiation zone were utilized in all subsequent analysis.

It can be seen from our data that the most significant change in the irradiated samples as compared to pristine samples was the formation of a shoulder at 286.2 eV (peak 3) accompanied by a decrease in the double peaks at 284.5 eV and 285 eV (peaks 1 and 2). As Table 1 indicates, the binding energy of 286.2 eV corresponds to aromatic C-O bonds while the peaks at 284.5 eV and 285 eV correspond to aromatic C-C/C-H and aliphatic C-C/C-H, respectively. This observation is consistent with several other studies about irradiation effects in polycarbonate which are discussed below (*36*, *42*, *43*, *44*, *45*, *46*). For the analysis presented in the next section, we focus on the peaks 1-6, as the satellite features (peaks 7-8) offer no additional information and are discussed in detail elsewhere (*47*).

3. Results and discussion

Here we discuss both the qualitative and quantitative trends observed in these irradiation data. First, the enhanced shoulder formation seen in our data at 286.2 eV (peak 3) is attributed to the formation of carbon-oxygen bonds and was reported elsewhere under Ar^{1+} irradiation with kinetic energies ranging from 0.5 keV to 1.5 keV and fluences of $10^{15} - 10^{16}$ cm^{-2} (*48*). Those singly charged ion irradiations, however, were accompanied by the simultaneous application of an oxygen gas flow across the sample. Hence, these prior results were described using a two-step model where bond breaking due to the irradiation leads to chemically active dangling bonds that react with the flowing oxygen to form C-O which appears as a shoulder in the XPS spectra. This interpretation was reinforced by the fact that the singly charged ion irradiation *without* the oxygen gas flow resulted in *no* discernible change in the chemical composition of the polycarbonate samples. Our data taken with MCIs and without oxygen gas flow runs counter to this particular model and, moreover, shows that the effects are initiated at a significantly lower (3 orders of magnitude) fluence when compared with singly charged ions. In both the current measurements and those of Ref. (*48*), however, the authors note that samples were removed from the irradiation environment and exposed to ambient conditions prior to their analyses. While both cases appear to preserve aspects of the irradiation effects, a more thorough investigation of the role that these atmospheric exposures play appears necessary.

A more quantitative examination of our results is presented in Figure 3, which shows the relative contributions of the C-C, C-O, and C = O peaks to the measured XPS spectra as a function of the multicharged Ar and O ion fluence. In relation to Figure 2 and Table 1, these correspond to C-C (peaks 1-2), C-O (peaks 3,4,6) and C = O (peaks 4,5,6), where the scaled contributions of peaks 4 and 6 in the C-O and C = O case are accounted for. In both the Ar and O ion cases, there is only a small decrease in the C-C contribution across the investigated fluence range, whereas the C-O component grows by more than a factor of three. This figure also shows that there is a significant enhancement in the carbonate (C = O) contribution to the XPS spectra.

In order to interpret these data for MCIs, we first note that the low ion kinetic energies ensure a shallow penetration depth into the polycarbonate target. This was verified using SRIM where ranges for Ar and O ions on polycarbonate were calculated to be 5 nm and 3 nm, respectively (*49*). Charge state effects on stopping power and range are currently not included in the SRIM code, and it has been shown that charge-state dependent stopping power is an open question (*50*). For example, enhanced pre-equilibrium stopping effects

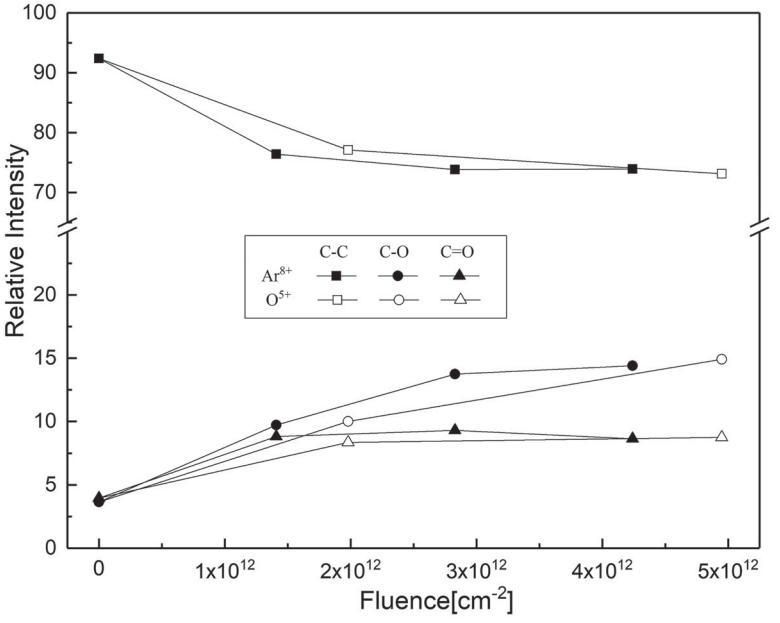

Figure 3. The relative intensities for different bond types at the polycarbonate surface as extracted from XPS spectra. The data are for O^{5+} and Ar^{8+} ion irradiations as a function of fluence.

for multicharged ions may lead to a charge-state dependent increase in stopping power (*51*, *52*). Therefore, we can consider the ranges obtained from SRIM to be an upper bound for the range of our multicharged ion at the same kinetic energy. The shallow penetration depths for our ions is not sufficient to explain the mismatch between their low fluence and the observed damage on the polycarbonate surface, and we propose that the ion charge state plays a role in facilitating the ion-induced damage.

For MCIs there is a well-known 'over-the-barrier' interpretation of their interaction with targets which defines a critical radius, $R_c = \frac{\sqrt{2Q}}{W}$, at which an impinging ion can capture a surface electron, where Q is the ion charge state and W is the surface work function (both in atomic units). If one considers that electron extraction by MCIs is one of the primary differences between them and singly charged ions, then one should envision a partially neutralized MCI at the surface having a range of interaction for charge extraction that is both Q-dependent and that extends well beyond that observed for an SCI. That this is the case can be seen in the damage estimates obtained from data on other samples, such as ionic crystals and two dimensional materials, see e.g. Refs. (*53*, *54*). In these cases, regions touched by the MCI interaction can be as high as a few hundred nm^2, or well beyond the typical cross sections for singly charged ions ($\sim 10^{-16}\,cm^{-2}$). In fact, those results from other targets far exceed what would be needed to match the observed enhancements we see here between MCI and SCI irradiations on polycarbonate, i.e. $2\text{-}5\times10^{-14}\,cm^{-2}$. We note also that it not merely the charge extraction, but also the secondary reionization and deexcitation steps as well as the collision of the ion itself that must be considered to capture a full picture of what occurs during the MCI-surface collision. Therefore, we take our result merely as evidence that irradiation and surface processing with multicharged ions can provide a

charge-dependent or *Q*-effect that enhances bond breaking at a polycarbonate surface at a level well beyond that seen with singly charged species.

It is useful to compare our results to those obtained at higher energies, where pore data have been obtained (*32*, *33*, *34*, *35*). In the majority of these works, the focus was on the etching rates for pores that were created as a result of the MCI irradiation, with scanning electron microscopy, scanning tunneling microscopy or foil resistance as the probing method. In all cases, relatively large initial pore sizes can be extracted from the data and are in the ranges of 7-75 nm. These all significantly exceed the interaction radii one would expect based on the cross sections we observe here, albeit with much lower charge states. One source of this difference could be the fundamental limits imposed by the etching methods and the need for significant post-processing, in the case of tunneling microscopy. What these data do point to, however, is an interpretation of the track regions around MCI-created pores in PC that include a 'core region' and 'halo' region, which are on the order of 10 nm and 20-200 nm, respectively. In addition, one of these studies utilized Ag, Cu and Si at charge states more consistent with our work ($q = 1-3$) that shows a result that indicates that the initial pore size increases with incident charge state (*35*). While this was not the focus of that work, it is consistent with what we have seen here, i.e. an increased interaction area at the surface with the higher MCI charge state.

4. Conclusion

We have shown that multicharged ion irradiation of polycarbonate targets results in a significant enhancement in surface modification relative to singly charged ions. Specifically, XPS analysis shows evidence of bond-breaking at the polycarbonate surface that far exceeds that seen for state-of-the-art ion processing of these materials. Also, the observed effects occur without the presence of a secondary flow of oxygen during the irradiation and therefore do not conform to a two-step model used in this field. The effective damage per ion we observe is well below that seen for slow multicharged ion irradiations of oxide and two-dimensional targets; however, the enhanced effects indicate that the charge state does play a role. In addition, our results are consistent with polycarbonate data focused on pore formation, which indicate an initial pore size that grows with the incident charge state.

Disclosure statement

No potential conflict of interest was reported by the authors.

Funding

Defense Advanced Research Projects Agency W911NF-13-1-0042

ORCID

E. S. Srinadhu http://orcid.org/0000-0001-7369-1568
J. E. Harriss http://orcid.org/0000-0002-0892-9653
C. E. Sosolik http://orcid.org/0000-0001-6686-2584

References

(1) Park, S.C.; Koh, S.K.; Pae, K.D. *Polym. Eng. Sci.* **1998,** *38,* 1185–1192.

(2) Lee, J.H.; Cho, J.S.; Koh, S.K.; Kim, D. *Thin Solid Films* **2004,** *449,* 147–151.
(3) Gnaser, H.; Heinz, B.; Bock, W.; Oechsner, H. *Phys. Rev. B* **1995,** *52,* 14086–14092.
(4) Shenton, M.J.; Bradley, J.W.; van den Berg, J.A.; Armour, D.G.; Stevens, G.C. *J. Phys. Chem. B* **2005,** *109,* 22085–22088.
(5) Echenique, P.; de Abajo, F.G.; Ponce, V.; Uranga, M. *Nucl. Instrum. Methods Phys. Res. Sect. B: Beam Interact. Mater. Atoms* **1995,** *96,* 583–603.
(6) Los, J.; Geerlings, J.J.C. *Phys. Rep.* **1990,** *190,* 133–190.
(7) Burgdorfer, J. Chap. Atomic Collisions with Surfaces. In *Review of Fundamental Processes and Applications of Atoms and Ions*; Lin C. D., Eds.; World Scientific Publishing Co. Pte. Ltd.: New Jersey, 1993; pp 517.
(8) Winter, H. *Phys. Rep.* **2002,** *367,* 387–582.
(9) Heiland, W. Chap. Interaction of Low-Energy Ions, Atoms and Molecules with Surfaces. In *Interaction of Charged Particles with Solids and Surfaces* Gras-Marti, A., Urbassek, H. M., Arista, N. R., Flores, F., Eds.; Plenum Press: New York, 1991; p 253.
(10) Goebl, D.; Roth, D.; Primetzhofer, D.; Monreal, R.C.; Abad, E.; Putz, A.; Bauer, P. *J. Phys.: Condens. Matter* **2013,** *25,* 485006.
(11) Kim, H.K.; Titze, J.; Schöffler, M.; Trinter, F.; Waitz, M.; Voigtsberger, J.; Sann, H.; Meckel, M.; Stuck, C.; Lenz, U.; Odenweller, M.; Neumann, N.; Schössler, S.; Ullmann-Pfleger, K.; Ulrich, B.; Fraga, R.C.; Petridis, N.; Metz, D.; Jung, A.; Grisenti, R.; Czasch, A.; Jagutzki, O.; Schmidt, L.; Jahnke, T.; Schmidt-Böcking, H.; Dörner, R. *Proc. Natl. Acad. Sci.* **2011,** *108,* 11821–11824.
(12) Krok, F.; Kolodziej, J.; B., S.; Czuba, P.; Piatkowski, P.; Struski, P.; Szymonski, M. *Nucl. Instrum. Methods Phys. Res. B* **2004,** *226,* 601–608.
(13) Takahashi, S.; Nagata, K.; Tona, M.; Sakurai, M.; Nakamura, N.; Yamada, C.; Ohtani, S. *Surf. Sci.* **2005,** *593,* 318–323.
(14) Burgdorfer, J.; Yamazaki, Y. *Phys. Rev. A* **1996,** *54,* 4140–4144.
(15) Kakutani, N.; Azuma, T.; Yamazaki, Y.; Komaki, K.; Kuroki, K. *Nucl. Instrum. Methods Phys. Res. B* **1995,** *96,* 541–544.
(16) Yamazaki, Y.; Kuroki, K. *Curr. Opin. Solid State Mater. Sci.* **2002,** *6,* 169–179.
(17) Gillaspy, J.D.; Pomeroy, J.M.; Perrella, A.C.; Grube, H. *J. Phys.: Conf. Ser.* **2007,** *58,* 451–456.
(18) Varga, P.; Neidhart, T.; Sporn, M.; Libiseller, G.; Schmid, M.; Aumayr, F.; Winter, H.P. *Phys. Scripta* **1997,** *T73,* 307–310.
(19) Aumayr, F.; El-Said, A.; Meissl, W. *Nucl. Instrum. Methods Phys. Res. Section B: Beam Interact. Mater. Atoms* **2008,** *266,* 2729–2735.
(20) Gebeshuber, I.; Cernusca, S.; Aumayr, F.; Winter, H. *Int. J. Mass Spectrom.* **2003,** *229,* 27–34.
(21) El-Said, A.; Heller, R.; Meissi, W.; Facsko, S.; Lemell, C.; Solleder, B.; Gebeshuber, I.; Betz, G.; Toulemonde, M.; Moller, W.; Burgdorfer, J.; Aumayr, F. *Phys. Rev. Lett.* **2008,** *100,* 237601.
(22) Ritter, R.; Wilhelm, R.; Stoger-Pollach, M.; Heller, R.; Mucklich, A.; Werner, U.; Vieker, H.; Beyer, A.; Facsko, S.; Golzhauser, A.; Aumayr, F. *Appl. Phys. Lett.* **2013,** *102,* 0632112.
(23) Borsoni, G.; Roux, V.L.; Laffitte, R.; Kerdilés, S.; Béchu, N.; Vallier, L.; Korwin-Pawlowski, M.; Vannuffel, C.; Bertin, F.; Vergnaud, C.; Chabli, A.; Wyon, C. *Solid-State Electron.* **2002,** *46,* 1855–1862.
(24) Fink, D.; Alegaonkar, P.; Petrov, A.; Wilhelm, M.; Szimkowiak, P.; Behar, M.; Sinha, D.; Fahrner, W.; Hoppe, K.; Chadderton, L. *Nucl. Instrum. Methods Phys. Res. Section B: Beam Interact. Mater. Atoms* **2005,** *236,* 11–20.
(25) Apel, P. *Nucl. Instrum. Methods Phys. Res. Section B: Beam Interact. Mater. Atoms* **2003,** *208,* 11–20.
(26) Facsko, S.; Heller, R.; El-Said, A.S.; Meissl, W.; Aumayr, F. *J. Phys.: Condens. Matter* **2009,** *21,* 224012.
(27) Tona, M.; Takahashi, S.; Nagata, K.; Yoshiyasu, N.; Yamada, C.; Nakamura, N.; Ohtani, S.; Sakurai, M. *Appl. Phys. Lett.* **2005,** *87,* 224102.
(28) Neidhart, T.; Pichler, F.; Aumayr, F.; Winter, H.; Schmid, M.; Varga, P. *Phys. Rev. Lett.* **1995,** *74,* 5280–5283.
(29) Aumayr, P.V.F.; Burgdörfer, J.; Winter, H. *Comments At. Mol. Phys.* **1999,** *34,* 210.
(30) Aumayr, F.; Varga, P.; Winter, H. *Int. J. Mass Spectrom.* **1999,** *192,* 415–424.
(31) Sporn, M.; Libiseller, G.; Neidhart, T.; Schmid, M.; Aumayr, F.; Winter, H.; Varga, P.; Grether, M.; Niemann, D.; Stolterfoht, N. *Phys. Rev. Lett.* **1997,** *79,* 945–948.
(32) Apel, P. *Nucl. Tracks Radiat. Meas.* **1991,** *19,* 29–34.

(33) Kemmer, H.; Grafström, S.; Neitzert, M.; Wörtge, M.; Neumann, R.; Trautmann, C.; Vetter, J.; Angert, N. *Ultramicroscopy* **1992,** *42-44,* 1345–1349.
(34) Petersen, F.; Enge, W. *Radiat. Meas.* **1995,** *25,* 43–46.
(35) Chen, Y.; Zhao, Z.; Dai, J.; Liu, Y.; Ma., H.; Nie, R. *Radiat. Meas.* **2008,** *43,* S111–S115.
(36) Muir, B.W.; Mc Arthur, S.L.; Thissen, H.; Simon, G.P.; Griesser, H.J.; Castner, D.G. *Surf. Interface Anal.* **2006,** *38,* 1186–1197.
(37) Choi, W.; Koh, S.; Jung, H. *J. Vac. Sci. Technol. A: Vac. Surf. Films* **1996,** *14,* 2366–2371
(38) Cho, J.S.; Choi, W.K.; Jung, H.J.; Koh, S.K.; Yoon, K.H. *J. Mater. Res.* **1997,** *12,* 277–282
(39) Takaoka, G.H.; Ryuto, H.; Araki, R.; Yakushiji, T. *AIP Conf. Proc.* **2008,** *1066,* 240.
(40) Koh, S.K.; Choi, W.K.; Cho, J.S.; Song, S.K.; Kim, Y.M.; Jung, H.J. *J. Mater. Res.* **1996,** *11,* 2933–2939.
(41) Shyam, R.; Kulkarni, D.D.; Field, D.A.; Srinadhu, E.S.; Cutshall, D.B.; Harrell, W.R.; Harriss, J.E.; Sosolik, C.E. *AIP Conf. Proc.* **2015,** *1640,* 129.
(42) Srivastava, A.; Singh, T.V.; Mule, S.; Rajan, C.R.; Ponrathnam, S. *Nucl. Instrum. Methods Phys. Res. Section B-Beam Interact. Mater. Atoms* **2002,** *192,* 402–406.
(43) Poirier, A.; Ross, G.G.; Bertrand, P.; Wiertz, V. *MRS Proc.* **1997,** *504,* 425.
(44) Poirier, A.; Ross, G. *Proc. SPIE* **1998,** *3413,* 235.
(45) Dehaye, F.; Balanzat, E.; Ferain, E.; Legras, R. *Nucl. Instrum. Methods Phys. Res. Section B-Beam Interact. Mater. Atoms* **2003,** *209,* 103–112.
(46) Goyal, P.K.; Kumar, V.; Gupta, R.; Mahendia, S.; Anita, ; Kumar, S. *Vacuum* **2012,** *86,* 1087–1091.
(47) Srinadhu, E. Ph. D. thesis, Clemson University, 2016.
(48) Cho, J.S.; Choi, W.K.; Jung, H.J.; Koh, S.K.; Yoon, K.H. *J. Mater. Res.* **1997,** *12,* 277–282.
(49) Ziegler, J.F.; Ziegler, M.D.; Biersack, J.P. *Nucl. Instrum. Methods Phys. Res. Section B-Beam Interact. Mater. Atoms* **2010,** *268,* 1818–1823.
(50) Kulkarni, D.D.; Shyam, R.E.; Cutshall, D.B.; Field, D.A.; Harriss, J.E.; Harrell, W.R.; Sosolik, C.E. *J. Mater. Res.* **2015,** *30,* 1413–1421.
(51) Brandt, W.; Kitagawa, M. *Phys. Rev. B* **1982,** *25,* 5631–5637.
(52) Wilhelm, R.A.; Gruber, E.; Ritter, R.; Heller, R.; Facsko, S.; Aumayr, F. *Phys. Rev. Lett.* **2014,** *112,* 153201.
(53) Wilhelm, R.; El-Said, A.; Krok, F.; Heller, R.; Gruber, E.; Aumayr, F.; Facsko, S. *Prog. Surf. Sci.* **2015,** *90,* 377–395.
(54) Aumayr, F.; Facsko, S.; El-Said, A.; Trautmann, C.; Schleberger, M. *J. Phys.: Condens. Matt.* **2011,** *23,* 393001.